Solutions of large-scale electromagnetics problems involving dielectric objects with the parallel multilevel fast multipole algorithm

Özgür Ergül

Department of Mathematics and Statistics, University of Strathclyde, G11XH Glasgow, UK, ozgur.ergul@strath.ac.uk

Received June 28, 2011; revised September 8, 2011; accepted September 8, 2011; posted September 12, 2011 (Doc. ID 150015); published October 11, 2011

Fast and accurate solutions of large-scale electromagnetics problems involving homogeneous dielectric objects are considered. Problems are formulated with the electric and magnetic current combined-field integral equation and discretized with the Rao–Wilton–Glisson functions. Solutions are performed iteratively by using the multilevel fast multipole algorithm (MLFMA). For the solution of large-scale problems discretized with millions of unknowns, MLFMA is parallelized on distributed-memory architectures using a rigorous technique, namely, the hierarchical partitioning strategy. Efficiency and accuracy of the developed implementation are demonstrated on very large problems involving as many as 100 million unknowns.

OCIS codes: 290.0290, 230.5298.

1. INTRODUCTION

Real-life electromagnetics problems, such as scattering from red blood cells [1] and transmission through lens systems and photonic crystals [2], often involve large objects, whose accurate numerical solutions require dense discretizations with large numbers of unknowns. Fast methods, such as the multilevel fast multipole algorithm (MLFMA) [3–5], have been proposed to efficiently and accurately solve these large-scale problems. Using MLFMA, matrix-vector multiplications required for iterative solutions can be performed in $\mathcal{O}(N \log N)$ time using $\mathcal{O}(N \log N)$ memory for dense matrix equations involving $\mathcal{O}(N)$ unknowns. Although MLFMA running on a single processor can be sufficient to solve a variety of problems, parallelization of this algorithm on multiprocessor computers is essential to enable the solution of very large problems. Recently, various parallelization techniques have been developed and implemented [5–16], increasing the problem size from millions to more than 1 billion. On the other hand, those implementations have been designed for perfectly-conducting objects and less attention has been paid to more general problems involving dielectric structures [11,12].

This paper present an efficient parallelization of MLFMA for the solution of large-scale problems involving three-dimensional homogeneous dielectric objects. The problems are formulated with the electric and magnetic current combined-field integral equation (JMCFIE) [17–20] and discretized with the Rao–Wilton–Glisson (RWG) [21] functions on planar triangles. The resulting dense matrix equations are solved iteratively by using a parallel implementation of MLFMA on distributed-memory architectures. A rigorous parallelization technique, namely, the hierarchical partitioning strategy [8,13], is used for the efficient parallelization of multilevel tree structures. The developed implementation is employed to solve dielectric problems involving more than 100 million unknowns on moderate parallel computers. The numerical results, some of which are presented in this paper, can be used for benchmarking purposes, e.g., to test the accuracy of approximate high-frequency techniques.

The rest of the paper is organized as follows. Section 2 summarizes matrix equations obtained from discretizations of electromagnetics problems formulated with JMCFIE. Application of MLFMA to JMCFIE is discussed in Section 3. Section 4 presents efficient parallelization of the implementation using the hierarchical strategy, followed by numerical results in Section 5, and concluding remarks in Section 6. Time-harmonic electromagnetic fields with the $e^{-i\omega t}$ time dependence are assumed throughout the paper.

2. MATRIX EQUATIONS OBTAINED FROM JMCFIE

Discretizations of surface integral equations using a set of testing functions $\boldsymbol{t}_m$ and a set of basis functions $\boldsymbol{b}_n$ for m, $n = 1, 2, \ldots, N$ lead to $2N \times 2N$ dense matrix equations in the form of

$$\begin{bmatrix} \bar{\boldsymbol{Z}}^{(11)} & \bar{\boldsymbol{Z}}^{(12)} \\ \bar{\boldsymbol{Z}}^{(21)} & \bar{\boldsymbol{Z}}^{(22)} \end{bmatrix} \cdot \begin{bmatrix} \boldsymbol{x} \\ \boldsymbol{y} \end{bmatrix} = \begin{bmatrix} \boldsymbol{v} \\ \boldsymbol{w} \end{bmatrix}, \qquad (1)$$

where $\bar{\boldsymbol{Z}}^{(ab)}$ for a, $b = 1, 2$ are $N \times N$ matrix partitions. In (1), $\boldsymbol{x}$ and $\boldsymbol{y}$ represent vectors of N elements involving coefficients to expand the equivalent electric and magnetic currents, respectively. Using a Galerkin scheme, the basis and testing functions are identical. For JMCFIE, matrix elements, i.e., interactions of the basis and testing functions, are derived as

$$Z_{mn}^{(11)} = \alpha \int_{S_m} \mathrm{d}\boldsymbol{r}\, \boldsymbol{t}_m(\boldsymbol{r}) \cdot (\mathcal{T}_o + \mathcal{T}_i)\{\boldsymbol{b}_n\}(\boldsymbol{r}) + (1-\alpha) \int_{S_m} \mathrm{d}\boldsymbol{r}\, \boldsymbol{t}_m(\boldsymbol{r}) \cdot \hat{\boldsymbol{n}} \times (\mathcal{K}_o - \mathcal{K}_i)\{\boldsymbol{b}_n\}(\boldsymbol{r}) - (1-\alpha) \int_{S_m} \mathrm{d}\boldsymbol{r}\, \boldsymbol{t}_m(\boldsymbol{r}) \cdot \boldsymbol{b}_n(\boldsymbol{r}), \quad (2)$$

$$Z_{mn}^{(12)} = (1-\alpha) \int_{S_m} \mathrm{d}\boldsymbol{r}\, \boldsymbol{t}_m(\boldsymbol{r}) \cdot \hat{\boldsymbol{n}} \times (\eta_o^{-1}\mathcal{T}_o - \eta_i^{-1}\mathcal{T}_i)\{\boldsymbol{b}_n\}(\boldsymbol{r}) - \alpha \int_{S_m} \mathrm{d}\boldsymbol{r}\, \boldsymbol{t}_m(\boldsymbol{r}) \cdot (\eta_o^{-1}\mathcal{K}_o + \eta_i^{-1}\mathcal{K}_i)\{\boldsymbol{b}_n\}(\boldsymbol{r}) - \frac{1}{2}\alpha(\eta_o^{-1} - \eta_i^{-1}) \int_{S_m} \mathrm{d}\boldsymbol{r}\, \boldsymbol{t}_m(\boldsymbol{r}) \cdot \hat{\boldsymbol{n}} \times \boldsymbol{b}_n(\boldsymbol{r}), \quad (3)$$

$$Z_{mn}^{(21)} = -(1-\alpha) \int_{S_m} \mathrm{d}\boldsymbol{r}\, \boldsymbol{t}_m(\boldsymbol{r}) \cdot \hat{\boldsymbol{n}} \times (\eta_o\mathcal{T}_o - \eta_i\mathcal{T}_i)\{\boldsymbol{b}_n\}(\boldsymbol{r}) + \alpha \int_{S_m} \mathrm{d}\boldsymbol{r}\, \boldsymbol{t}_m(\boldsymbol{r}) \cdot (\eta_o\mathcal{K}_o + \eta_i\mathcal{K}_i)\{\boldsymbol{b}_n\}(\boldsymbol{r}) + \frac{1}{2}\alpha(\eta_o - \eta_i) \int_{S_m} \mathrm{d}\boldsymbol{r}\, \boldsymbol{t}_m(\boldsymbol{r}) \cdot \hat{\boldsymbol{n}} \times \boldsymbol{b}_n(\boldsymbol{r}), \quad (4)$$

where $\alpha \in [0, 1]$ is a combination parameter [18], $\hat{\boldsymbol{n}}$ is the unit normal vector at the observation point $\boldsymbol{r}$, and $\eta_u = \sqrt{\mu_u/\epsilon_u}$ represents the intrinsic impedance of the outer $(u = o)$ and inner $(u = i)$ media. The diagonal partitions are identical, i.e., $\bar{\boldsymbol{Z}}^{(11)} = \bar{\boldsymbol{Z}}^{(22)}$ in (1). The integro-differential operators can be applied to the nth basis function as

$$\mathcal{T}_u\{\boldsymbol{b}_n\}(\boldsymbol{r}) = ik_u \int_{S_n} \mathrm{d}\boldsymbol{r}'\, \boldsymbol{b}_n(\boldsymbol{r}') g_u(\boldsymbol{r}, \boldsymbol{r}') + \frac{i}{k_u} \int_{S_n} \mathrm{d}\boldsymbol{r}'\, \nabla' \cdot \boldsymbol{b}_n(\boldsymbol{r}') \nabla g_u(\boldsymbol{r}, \boldsymbol{r}'), \quad (5)$$

$$\mathcal{K}_u\{\boldsymbol{b}_n\}(\boldsymbol{r}) = \int_{\mathrm{PV}, S_n} \mathrm{d}\boldsymbol{r}'\, \boldsymbol{b}_n(\boldsymbol{r}') \times \nabla' g_u(\boldsymbol{r}, \boldsymbol{r}'), \quad (6)$$

where PV indicates the principal value of the integral, $k_u = \omega\sqrt{\epsilon_u \mu_u}$ is the wavenumber, and

$$g_u(\boldsymbol{r}, \boldsymbol{r}') = \frac{\exp(ik_u|\boldsymbol{r} - \boldsymbol{r}'|)}{4\pi|\boldsymbol{r} - \boldsymbol{r}'|} \quad (7)$$

denotes the homogeneous-space Green's function. Elements of the right-hand-side vectors in (1) can be derived similarly as

$$v_m = -(1-\alpha) \int_{S_m} \mathrm{d}\boldsymbol{r}\, \boldsymbol{t}_m(\boldsymbol{r}) \cdot \hat{\boldsymbol{n}} \times \boldsymbol{H}^{\mathrm{inc}}(\boldsymbol{r}) - \alpha\eta_o^{-1} \int_{S_m} \mathrm{d}\boldsymbol{r}\, \boldsymbol{t}_m(\boldsymbol{r}) \cdot \boldsymbol{E}^{\mathrm{inc}}(\boldsymbol{r}), \quad (8)$$

$$w_m = (1-\alpha) \int_{S_m} \mathrm{d}\boldsymbol{r}\, \boldsymbol{t}_m(\boldsymbol{r}) \cdot \hat{\boldsymbol{n}} \times \boldsymbol{E}^{\mathrm{inc}}(\boldsymbol{r}) - \alpha\eta_o \int_{S_m} \mathrm{d}\boldsymbol{r}\, \boldsymbol{t}_m(\boldsymbol{r}) \cdot \boldsymbol{H}^{\mathrm{inc}}(\boldsymbol{r}), \quad (9)$$

where $\boldsymbol{E}^{\mathrm{inc}}$ and $\boldsymbol{H}^{\mathrm{inc}}$ are incident electric and magnetic fields created by external sources in the outer medium. In (2)–(9), S_m and S_n represent the spatial supports of the mth testing function $\boldsymbol{t}_m$ and the nth basis function $\boldsymbol{b}_n$, respectively.

3. MULTILEVEL FAST MULTIPOLE ALGORITHM

The matrix equation in (1) can be solved iteratively via a Krylov-subspace algorithm, where the required matrix-vector multiplications can be performed efficiently with MLFMA. Multilevel tree structures are constructed by placing the object in a cubic box and recursively dividing its surface into subdomains. Then, far-field interactions that are between distant basis and testing functions can be performed efficiently in three stages, namely, aggregation, translation, and disaggregation, using the factorization and diagonalization of the homogeneous-space Green's functions [5]. Different tree structures are required for the outer and inner media, since the sampling rate to compute far-field interactions depends on the wavenumber, hence the electrical parameters of the medium [19]. In an aggregation stage, radiated fields are calculated from the lowest level to the top of the tree structure. At the lowest level, the radiated field of a subdomain is obtained by combining radiation patterns of the basis functions located inside the subdomain. The radiation pattern of the nth basis function with respect to a reference point $\boldsymbol{r}_C$ is defined as

$$\boldsymbol{R}_n^{(u)}(\boldsymbol{r}_C, \boldsymbol{k}_u) = \gamma_n(\bar{\boldsymbol{I}} - \hat{\boldsymbol{k}}\hat{\boldsymbol{k}}) \cdot \boldsymbol{S}_n^{-}(\boldsymbol{r}_C, \boldsymbol{k}_u), \quad (10)$$

where $\bar{\boldsymbol{I}}$ is the 3×3 unit dyad, $\gamma_n = \pm 1$ represents the orientation of the basis function, and

$$\boldsymbol{S}_n^{-}(\boldsymbol{r}_C, \boldsymbol{k}_u) = \int_{S_n} \mathrm{d}\boldsymbol{r} \exp[-i\boldsymbol{k}_u \cdot (\boldsymbol{r} - \boldsymbol{r}_C)] \boldsymbol{b}_n(\boldsymbol{r}). \quad (11)$$

Radiated fields of subdomains at the higher levels are obtained by combining radiated fields of subdomains at the lower levels. Lagrange interpolation is used to change the sampling rate between the consecutive levels during the aggregation stage. In a translation stage, radiated fields of subdomains are converted into incoming fields for other subdomains at the same level. Finally, in a disaggregation stage, total incoming fields are calculated from the top of the tree structure to the lowest level. At the lowest level, total incoming fields are received by the testing functions. As opposed to radiation patterns of the basis functions, receiving patterns of the testing functions depend on the matrix partition, i.e.,

$$\boldsymbol{R}_m^{(11,u)}(\boldsymbol{r}_C, \boldsymbol{k}_u) = \boldsymbol{R}_m^{(22,u)}(\boldsymbol{r}_C, \boldsymbol{k}_u) = \alpha\gamma_m(\bar{\boldsymbol{I}} - \hat{\boldsymbol{k}}\hat{\boldsymbol{k}}) \cdot \boldsymbol{S}_m^{+}(\boldsymbol{r}_C, \boldsymbol{k}_u) - (1-\alpha)\hat{\boldsymbol{k}} \times \boldsymbol{S}_m^{\times n}(\boldsymbol{r}_C, \boldsymbol{k}_u), \quad (12)$$

$$\boldsymbol{R}_m^{(12,u)}(\boldsymbol{r}_C,\boldsymbol{k}_u) = (1-\alpha)\eta_u^{-1}(\bar{\boldsymbol{I}} - \hat{\boldsymbol{k}}\hat{\boldsymbol{k}})\cdot \boldsymbol{S}_m^{\times n}(\boldsymbol{r}_C,\boldsymbol{k}_u) + \alpha\gamma_m\eta_u^{-1}\hat{\boldsymbol{k}}\times \boldsymbol{S}_m^{+}(\boldsymbol{r}_C,\boldsymbol{k}_u), \tag{13}$$

$$\boldsymbol{R}_m^{(21,u)}(\boldsymbol{r}_C,\boldsymbol{k}_u) = -(1-\alpha)\eta_u(\bar{\boldsymbol{I}} - \hat{\boldsymbol{k}}\hat{\boldsymbol{k}})\cdot \boldsymbol{S}_m^{\times n}(\boldsymbol{r}_C,\boldsymbol{k}_u) - \alpha\gamma_m\eta_u\hat{\boldsymbol{k}}\times \boldsymbol{S}_m^{+}(\boldsymbol{r}_C,\boldsymbol{k}_u), \tag{14}$$

where $\gamma_m = \pm 1$ represents the orientation of the testing function and

$$\boldsymbol{S}_m^{+}(\boldsymbol{r}_C,\boldsymbol{k}_u) = \int_{S_m} \mathrm{d}\boldsymbol{r}\exp[i\boldsymbol{k}_u\cdot(\boldsymbol{r}-\boldsymbol{r}_C)]\boldsymbol{t}_m(\boldsymbol{r}), \tag{15}$$

$$\boldsymbol{S}_m^{\times n}(\boldsymbol{r}_C,\boldsymbol{k}_u) = \int_{S_m} \mathrm{d}\boldsymbol{r}\exp[i\boldsymbol{k}_u\cdot(\boldsymbol{r}-\boldsymbol{r}_C)]\boldsymbol{t}_m(\boldsymbol{r})\times\hat{\boldsymbol{n}}. \tag{16}$$

Considering the expressions in (10) and (12)–(14), only θ and ϕ components of $\boldsymbol{S}_m^{-}$, $\boldsymbol{S}_m^{+}$, and $\boldsymbol{S}_m^{\times n}$ are required. If the medium is lossless (and using the Galerkin scheme),

$$\boldsymbol{S}_m^{+}(\boldsymbol{r}_C,\boldsymbol{k}_u) = \{\boldsymbol{S}_m^{-}(\boldsymbol{r}_C,\boldsymbol{k}_u)\}^*, \tag{17}$$

where $*$ represents the complex-conjugate operation.

4. HIERARCHICAL PARALLELIZATION OF MLFMA

Consider a multilevel tree structure involving $(L+2) = \mathcal{O}(\log(k_u D))$ levels obtained by recursively dividing an object of size D. At level l from 1 to L, there are $N_l \approx 4^{(1-l)}N_1$ nonempty subdomains, where $N_1 = \mathcal{O}(N)$. For each subdomain, radiated and incoming fields are sampled at $S_l = 2(T_l+1)^2$ directions, where the truncation number T_l is determined by the excess bandwidth formula. In general, the number of samples increases by a factor of four from a level to the next upper level, i.e., $S_l \approx 4^{(l-1)}S_1$ with $S_1 = \mathcal{O}(1)$. Consequently, the computational cost of the lth level is

$$N_l S_l \approx 4^{(1-l)}N_1 4^{(l-1)}S_1 = N_1 S_1 = \mathcal{O}(N), \tag{18}$$

which is independent of l. For a general three-dimensional object, $k_u D = \mathcal{O}(\sqrt{N})$, $L = \mathcal{O}(\log N)$, and the overall cost of MLFMA is $\mathcal{O}(N\log N)$.

Efficient parallelization of MLFMA is a challenging task due to the complicated structure of this algorithm. Simple parallelization strategies based on distributing subdomains among processes are usually not efficient since they do not provide a well-balanced partitioning for the higher levels of tree structures [10]. Since all levels of MLFMA have equal importance with $\mathcal{O}(N)$ complexity, its efficient parallelization should consider the best partitioning for each level. Along this direction, parallelization of MLFMA can significantly be improved by using advanced techniques, such as the hybrid strategy [6,10] using different partitioning schemes for the lower and higher levels and the asynchronous strategy using dynamic partitioning of the workload among processes [11].

Another advanced technique developed recently is the hierarchical partitioning strategy [8,13], which is based on the simultaneous partitioning of subdomains and their fields at all levels. Considering the number of subdomains and the number of samples, the partitioning is adjusted for each level independently to obtain the best possible parallelization. It can be shown that the hierarchical strategy leads to efficient parallelization of MLFMA by improving the load-balancing, reducing the total amount of communications, and facilitating process arrangements in nonuniform platforms to minimize internode communications [13]. As shown in this paper, the hierarchical strategy can also be applied to dielectric problems such that the resulting implementation enables the analysis of large-scale objects discretized with tens of millions of unknowns on modest parallel computers. To the best of author's knowledge, the hierarchical strategy has been applied to dielectric problems only for two-dimensional objects [12].

Consider the partitioning of the lth level involving N_l subdomains, whose radiated and incoming fields are sampled at S_l directions. Using the hierarchical strategy, subdomains and their samples are divided into $p_{l,c}$ and $p_{l,s}$ partitions, respectively, where $p_{l,c}p_{l,s} = p$ is the total number of processes. Subdomains are partitioned according to their indices in the multilevel tree structure and considering the partitioning in the lower $(l-1)$ and higher $(l+1)$ levels, if they exist. Samples are partitioned similarly along the θ direction. In general, the ratio $p_{l,c}/p_{l,s}$ decreases from the lower levels to the higher levels, but the actual partitioning is determined by load-balancing algorithms considering various factors [22–24].

A. Aggregation

Since field samples are partitioned, the aggregation stage requires one-to-one communications between processes. Specifically, local interpolations that are performed by a process requires samples owned by some other processes. In general, each process exchanges data with at most two processes; secondary communications with other processes can be avoided by adjusting the partitioning accordingly. Communications are performed for all local subdomains, followed by the interpolation and shift operations to aggregate radiated fields. After all subdomains are processed, one-to-one data exchanges are required between pairs of processes, if the partitioning is different in the upper level $(l+1)$. Each process sends half of the field samples for each subdomain and receives a complementary data from the associated process.

B. Translation

Since subdomains are partitioned, one-to-one communications are also required during the translation stage. For these communications, each process is paired one by one with the other $p_{l,c}-1$ processes. Once a pairing is established, all related translations between the subdomains located at the two different processes are performed. In addition to those translations requiring communications, there are also intraprocess translations that can be performed in each process without any pairing and communication.

C. Disaggregation

The disaggregation stage is the reverse of the aggregation stage, i.e., the tree structure is traced from the highest level to the lowest level. For each subdomain, the total incoming field is obtained by combining incoming fields due to translations and the incoming field from the parent subdomain. At level l, disaggregations start with data exchanges between pairs of processes, if the partitioning needs to be modified, compared to the partitioning at level $(l+1)$. Then, all local subdomains are processed, i.e., incoming fields from parent subdomains are shifted and anterpolated. Similar to those performed during interpolations of the aggregation stage, one-to-one communications (with at most two processes for each process) are required between processes to deflate the local data produced by anterpolations.

Using a two-dimensional partitioning by distributing both subdomains and field samples, the hierarchical strategy provides a well-balanced distribution of the workload among processes. In the case of homogeneous dielectric objects, there are two different tree structures associated with the outer and inner media. The hierarchical strategy can be applied to these tree structures separately to achieve the best possible partitioning for both of them.

5. NUMERICAL RESULTS

For numerical solutions, surfaces are discretized with the RWG functions on $\lambda_o/10$ triangles, where $\lambda_o = 2\pi/k_o$ is the wavelength in the outer medium. All objects are located in free space. Problems are formulated with JMCFIE using $\alpha = 0.5$ and solved iteratively via parallel MLFMA. Both near-field and far-field interactions are computed with maximum 1% error. Iterative solutions are performed by the biconjugate-gradient-stabilized (BiCGStab) algorithm [25] accelerated with block-diagonal preconditioners [19]. Iterations are carried out until the residual error is reduced to below 0.005. Solutions are parallelized by using the hierarchical strategy on a cluster of Intel Xeon Nehalem quad-core processors with 2.80 GHz clock rate.

Figure 1 presents solutions of a scattering problem involving a dielectric sphere with a radius of 0.3 m at 20 GHz. The radius of the sphere corresponds to approximately $20\lambda_o$ and the problem is discretized with 2,925,708 unknowns. The relative permittivity of the sphere is 2.0 and it is illuminated by a plane wave propagating in the z direction with the electric

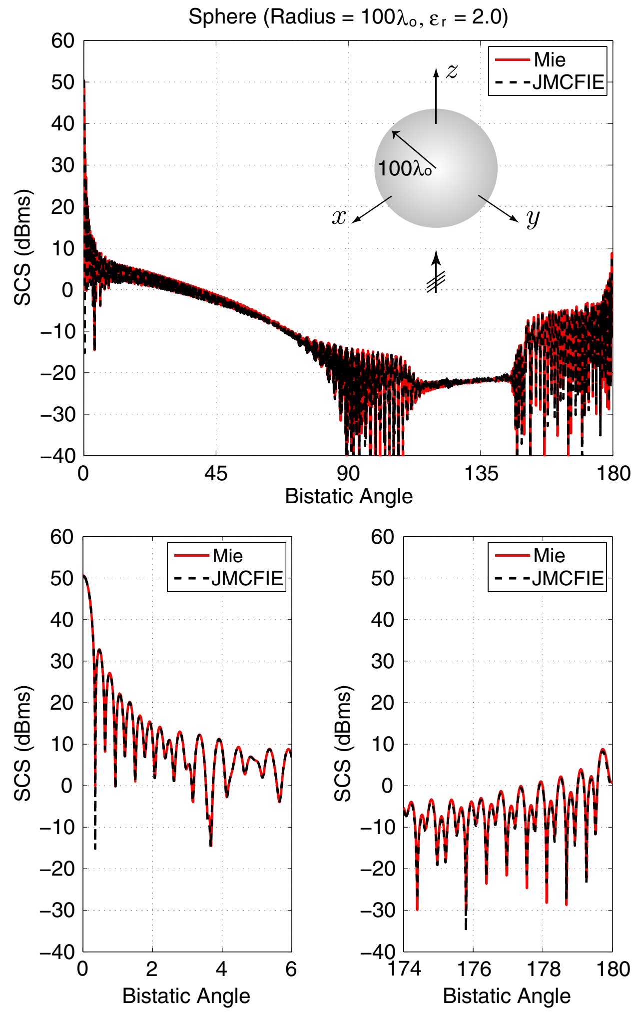

Fig. 2. (Color online) Solution of a scattering problem involving a dielectric sphere with a radius of 0.3 m at 100 GHz discretized with 67,582,464 unknowns. SCS (in dBms) is plotted as a function of the bistatic angle from 0° to 180°, where 0° and 180° correspond to the backscattering and forward-scattering directions, respectively. Computational values provided by the parallel MLFMA implementation agree well with the analytical Mie-series solution.

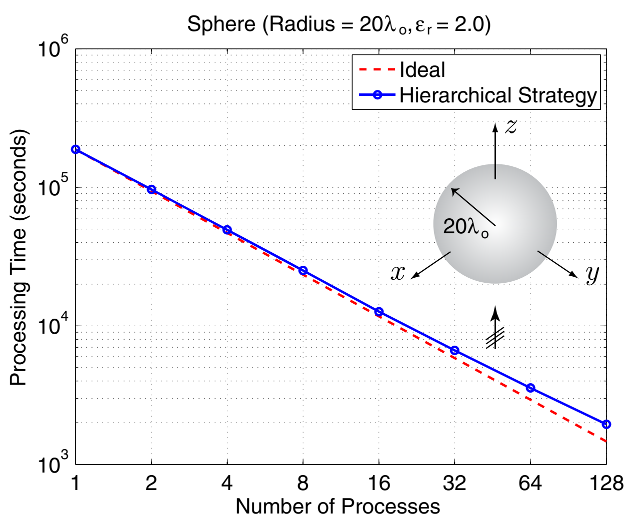

Fig. 1. (Color online) Solutions of a scattering problem involving a dielectric sphere with a radius of 0.3 m at 20 GHz discretized with 2,925,708 unknowns. The total computing time is plotted as a function of the number of processes from 1 to 128.

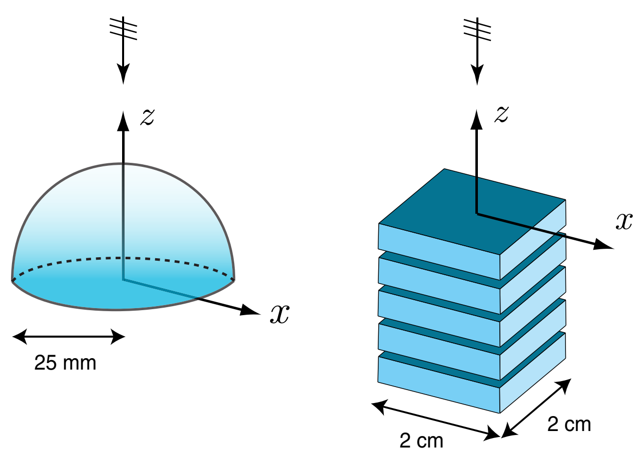

Fig. 3. (Color online) Electromagnetics problems involving a dielectric hemisphere lens with a radius of 25 mm and a periodic structure involving $2 \times 2 \times 0.41$ cm slabs (a simple photonic crystal). Both objects are illuminated by plane waves.

field polarized in the x direction. The solution requires 37 iterations. Figure 1 depicts the total time including the setup and iterations when the solution is parallelized into 2, 4, 8, 16, 32, 64, and 128 processes, in addition to the sequential solution (single process). The ideal case assuming 100% parallelization efficiency is also shown for comparisons. It can be observed that the computing time is significantly reduced from $t_1 = 187,516$ seconds to $t_{128} = 1947$ seconds when the number of processes is increased from 1 to 128. Hence, the parallelization efficiency is $(t_1/t_{128})/128 = 75\%$ on 128 processes, corresponding to 96-fold speedup, which is quite high, considering the difficult parallelization of MLFMA.

Figure 2 presents the solution of a scattering problem involving the same dielectric sphere (with 0.3 m radius and 2.0 relative permittivity) at 100 GHz. At this frequency, the radius of the sphere is approximately $100\lambda_o$ and the problem is discretized with 67,582,464 unknowns. The sphere is again illuminated by a plane wave propagating in the z direction with the electric field polarized in the x direction in free space. The solution of the problem, which is performed by using a 10-level MLFMA parallelized into 64 processes, requires 237 iterations and a total of 77 hours. The total amount of memory used for the solution is 723 GB. Figure 2 depicts the bistatic scattering cross section (SCS) values (in dBms) on the z-x plane as a function of the bistatic angle θ from 0° to 180°. Computational values obtained by using MLFMA are compared with those obtained via analytical Mie-series solutions. SCS values around the forward-scattering (0°) and backscattering (180°) directions are also focused in separate plots. It can be observed that the computational values agree well with the analytical results, confirming the high accuracy of the implementation even for very large problems.

In addition to the sphere, electromagnetics problems involving a dielectric hemisphere lens with a radius of 25 mm and a periodic structure involving $2 \times 2 \times 0.41$ cm slabs (a simple photonic crystal) are considered, as depicted in Fig. 3. The lens has a relative permittivity of 4.8 and it is illuminated by a plane wave propagating in the $-z$ direction (towards its convex surface). At 120 GHz and 1.08 THz, discretizations with $\lambda_o/10$ triangles lead to matrix equations involving 615,456

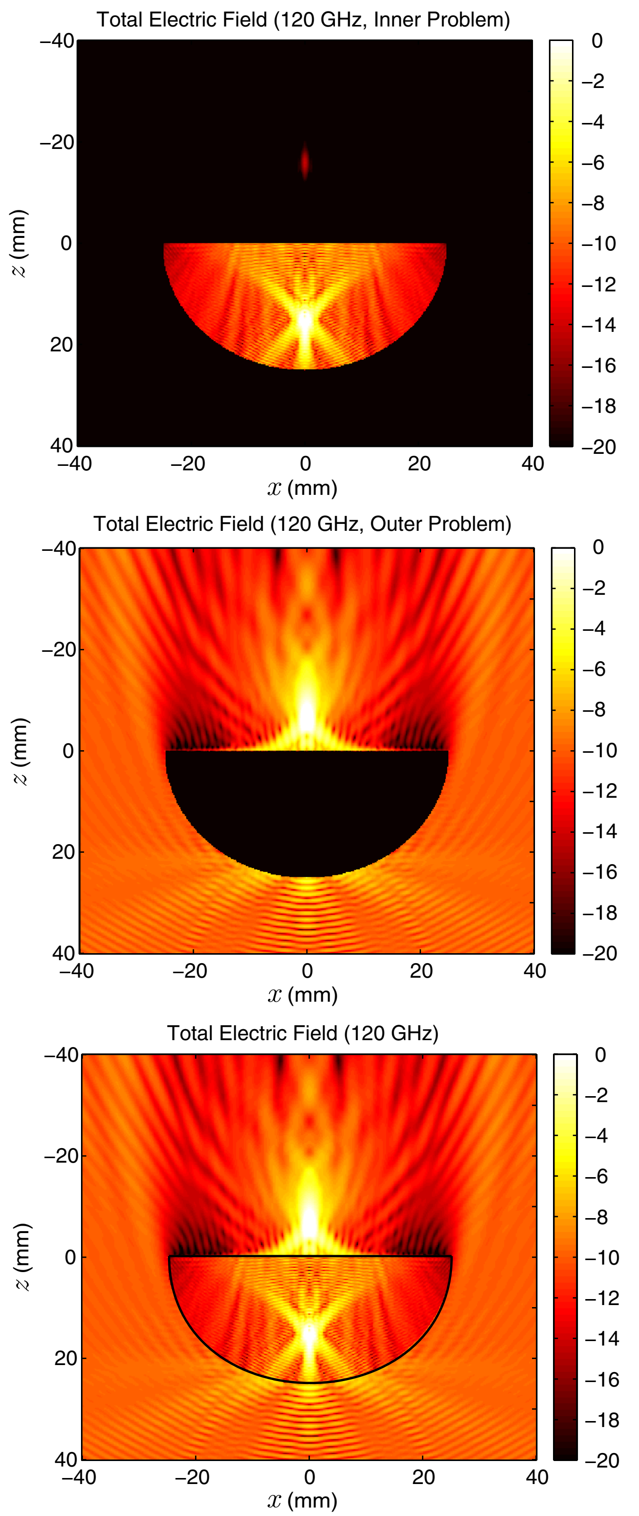

Fig. 4. (Color online) Solution of an electromagnetics problem involving a dielectric hemisphere lens with a radius of 25 mm at 120 GHz. The lens has a relative permittivity of 4.8 and the problem is discretized with 615,456 unknowns. The total electric field in the vicinity of the lens is plotted for the inner and outer problems, in addition to the complete plot obtained via their superposition.

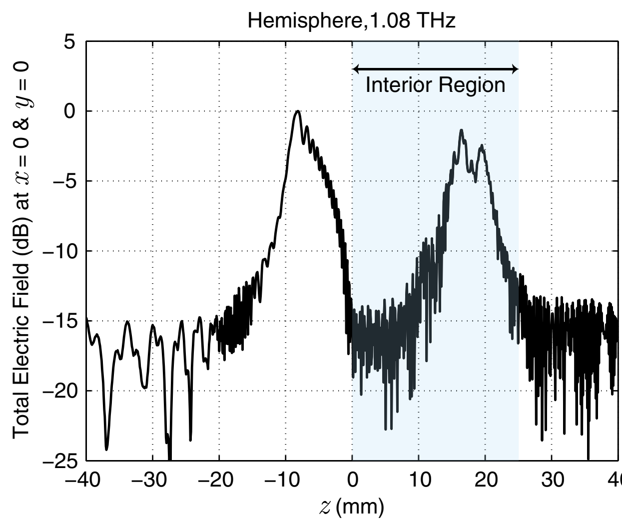

Fig. 5. (Color online) Solution of an electromagnetics problem involving a dielectric hemisphere lens with a radius of 25 mm at 1.08 THz. The lens has a relative permittivity of 4.8 and the problem is discretized with 49,851,936 unknowns. The total electric field on the axis of rotation of the lens is plotted from $z = -40$ mm to 40 mm.

and 49,851,936 unknowns, respectively. Figure 4 depicts the total electric field in the vicinity of the lens at 120 GHz. The solution at this frequency requires 48 iterations. Three different plots are shown in Fig. 4; the total electric field for the inner and outer problems and their superposition. For the inner problem, the equivalent currents obtained by MLFMA are allowed to radiate into a homogeneous space with the electrical parameters of the inner medium assumed everywhere. Hence, in this case, the equivalent currents should not radiate outside the object and any nonzero value can be interpreted as the error. As depicted in Fig. 4, the amplitude of the total electric field outside the object for the inner problem is below −20 dB, except for a tiny region. Similarly, for the outer problem, the equivalent currents radiate into a homogeneous space with the electric parameters of the outer medium and any radiation into the object can be interpreted as error. As also depicted in Fig. 4, the total electric field is below −20 dB inside the object for the outer problem, showing the high accuracy of the solution. Finally, by superposing the plots for the inner and outer problems, the complete plot in Fig. 4 can be obtained. In this plot, focusing due to the lens is clearly observed in the transmission region at around $z = -7$ mm, where the total electric field is maximum.

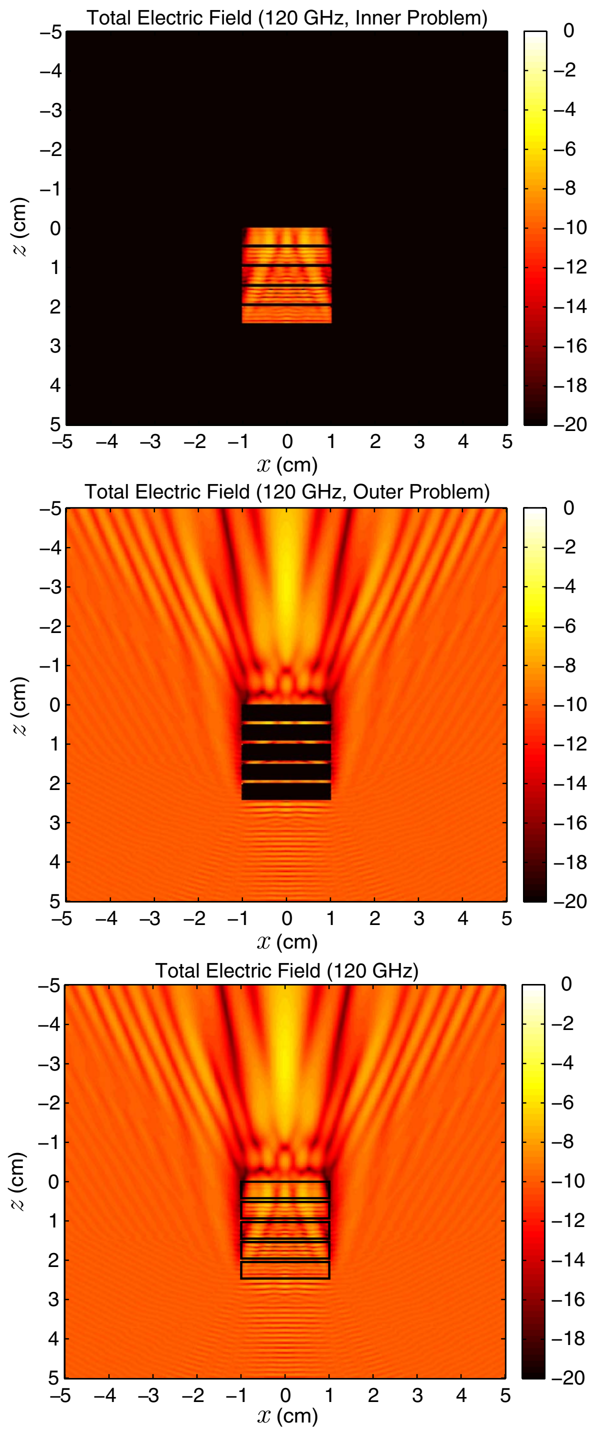

Fig. 6. (Color online) Solution of an electromagnetics problem involving five $2 \times 2 \times 0.41$ cm dielectric slabs at 120 GHz. The structure has a relative permittivity of 1.6 and the problem is discretized with 619,200 unknowns. The total electric field in the vicinity of the structure is plotted for the inner and outer problems, in addition to the complete plot obtained via their superposition.

Figure 5 presents the total electric field on the axis of rotation of the lens from $z = -40$ mm to 40 mm at 1.08 THz, i.e., when the radius of the hemisphere is approximately $90\lambda_o$. The solution of the problem involving 49,851,936 unknowns via 10-level MLFMA requires 105 iterations and a total of 19 hours using 128 processes. The total amount of memory used for the solution is 673 GB. Similar to the lower frequency case, a focussing is observed at around −7 mm.

Figures 6 and 7 present the solution of electromagnetics problems involving the simple photonic crystal depicted in Fig. 3. Five dielectric slabs of dimensions $2 \times 2 \times 0.41$ cm are placed at 0.5 cm intervals and illuminated by a plane wave. Scattering from this structure with 1.6 relative permittivity is investigated at 120 GHz and 1.62 THz. Discretizations at these frequencies lead to matrix equations involving 619,200 and 112,849,200 unknowns, respectively. Figure 6 presents the total electric field in the vicinity of the structure at 120 GHz. It can be observed that the unwanted radiations are below −20 dB for both the inner and outer problems. Figure 7 depicts

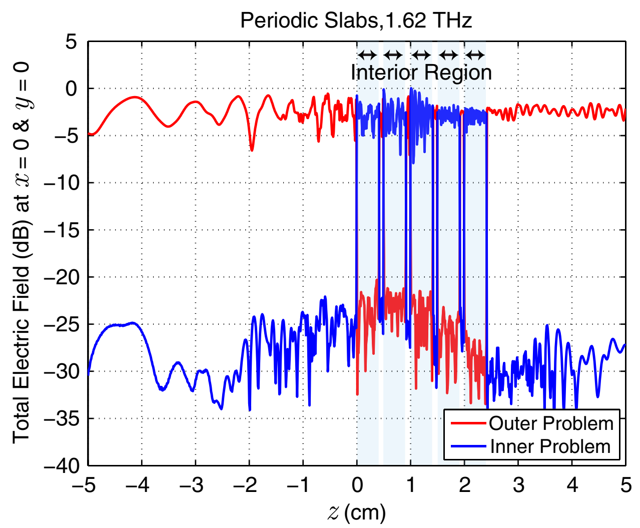

Fig. 7. (Color online) Solution of an electromagnetics problem involving five $2 \times 2 \times 0.41$ cm dielectric slabs at 1.62 THz. The structure has a relative permittivity of 1.6 and the problem is discretized with 112,849,200 unknowns. The total electric field on the axis of symmetry is plotted from $z = -5$ cm to 5 cm for the inner and outer problems.

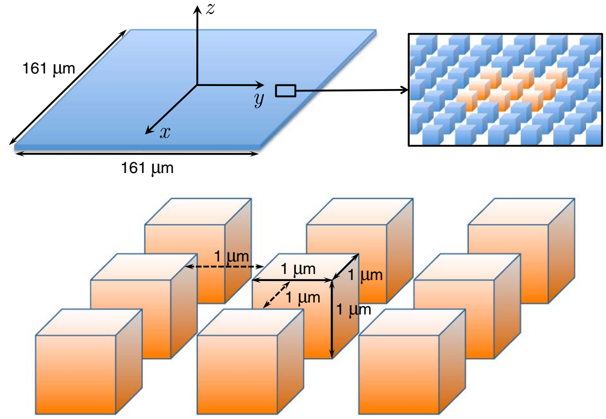

(a)

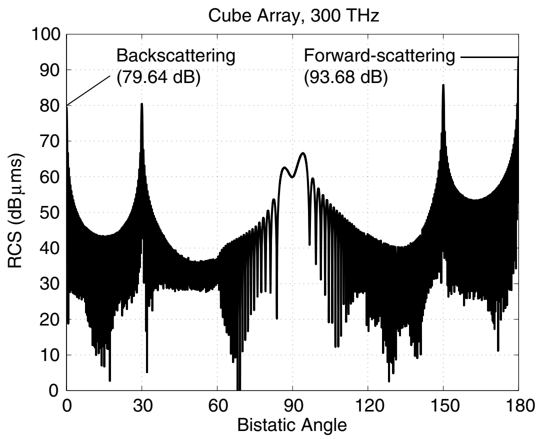

(b)

Fig. 8. (Color online) Solution of a scattering problem involving an array of $81 \times 81 = 6561$ lossy dielectric cubes. (a) Cubes with edges of $1\,\mu$m are periodically arranged on the x-y plane with $2\,\mu$m periodicity in both directions. The relative permittivity and conductivity of the cubes are 8.0 and 0.01 S/m, respectively. (b) SCS is plotted on the z-x plane, when the array is illuminated by a plane wave propagating in the $-z$ direction with the electric field polarized in the x direction at 300 THz.

the electric field on the axis of symmetry from $z = -5$ cm to 5 cm at 1.62 GHz. At this frequency, the solution of the problem via 10-level MLFMA requires 102 iterations and a total of 37 hours using 64 processes. The total amount of memory used for the solution is 669 GB. Similar to the previous results, investigation of the electric fields obtained for the inner and outer problems demonstrate the high accuracy of the solutions.

Finally, the solution of a scattering problem involving a two-dimensional array of $81 \times 81 = 6561$ lossy dielectric cubes is considered. As depicted in Fig. 8(a), cubes of edges $1\,\mu$m are periodically arranged on the x-y plane with $2\,\mu$m periodicity in both directions. The relative permittivity and conductivity of the cubes are 8.0 and 0.01 S/m, respectively. The array is illuminated by a plane wave propagating in the $-z$ direction with the electric field polarized in the x direction at 300 THz, i.e., when the edges of the cubes are approximately λ_o and the overall size of the structure is approximately $161\lambda_o \times 161\lambda_o \times \lambda_o$. The problem is discretized with 26,926,344 unknowns and solved in a total of nine hours (including 32 iterations) using 663 GB memory. Figure 8(b) depicts the bistatic SCS (in dB$\,\mu$m s) on the z-x plane, demonstrating peaks at around 30° and 150°, in addition to high values in the backscattering and forward-scattering directions.

6. CONCLUDING REMARKS

This paper presents a parallel implementation of MLFMA for rigorous solutions of large-scale electromagnetics problems involving three-dimensional dielectric objects. For efficient parallelization of MLFMA, the hierarchical partitioning strategy, which was developed for metallic objects, is extended to dielectric structures formulated with surface integral equations. The efficiency and accuracy of the resulting implementation are demonstrated on very large problems discretized with tens of millions of unknowns. In addition to showing the feasibility of full-wave solutions of large-scale dielectric problems, numerical results presented in this paper can be used for benchmarking purposes, e.g., testing the accuracy of implementations based on high-frequency techniques.

ACKNOWLEDGMENTS

This work was supported by the Centre for Numerical Algorithms and Intelligent Software (EPSRC EP/G036136/1) and the Research Starter Grant provided by the Faculty of Science at the University of Strathclyde. The author would like to thank Prof. Levent Gürel for fruitful discussions and making invaluable suggestions on this work.

REFERENCES

1. Ö. Ergül, A. Arslan-Ergül, and L. Gürel, "Computational study of scattering from healthy and diseased red blood cells using surface integral equations and the multilevel fast multipole algorithm," J. Biomed. Opt. **15**, 045004 (2010).
2. Ö. Ergül, T. Malas, and L. Gürel, "Analysis of dielectric photonic-crystal problems with MLFMA and Schur-complement preconditioners," J. Lightwave Technol. **29**, 888–897 (2011).
3. J. Song, C.-C. Lu, and W. C. Chew, "Multilevel fast multipole algorithm for electromagnetic scattering by large complex objects," IEEE Trans. Antennas Propag. **45**, 1488–1493 (1997).
4. X.-Q. Sheng, J.-M. Jin, J. Song, W. C. Chew, and C.-C. Lu, "Solution of combined-field integral equation using multilevel fast multipole algorithm for scattering by homogeneous bodies," IEEE Trans. Antennas Propag. **46**, 1718–1726 (1998).
5. W. C. Chew, J.-M. Jin, E. Michielssen, and J. Song, *Fast and Efficient Algorithms in Computational Electromagnetics* (Artech House, 2001).
6. S. Velamparambil, W. C. Chew, and J. Song, "10 million unknowns: Is it that big?" IEEE Trans. Antennas Propag. **45**, 43–58 (2003).
7. L. Gürel and Ö. Ergül, "Fast and accurate solutions of integral-equation formulations discretised with tens of millions of unknowns," Electron. Lett. **43**, 499–500 (2007).
8. Ö. Ergül and L. Gürel, "Hierarchical parallelisation strategy for multilevel fast multipole algorithm in computational electromagnetics," Electron. Lett. **44**, 3–5 (2008).
9. X.-M. Pan and X.-Q. Sheng, "A sophisticated parallel MLFMA for scattering by extremely large targets," IEEE Trans. Antennas Propag. **50**, 129–138 (2008).
10. Ö. Ergül and L. Gürel, "Efficient parallelization of the multilevel fast multipole algorithm for the solution of large-scale scattering problems," IEEE Trans. Antennas Propag. **56**, 2335–2345 (2008).
11. J. Fostier and F. Olyslager, "An asynchronous parallel MLFMA for scattering at multiple dielectric objects," IEEE Trans. Antennas Propag. **56**, 2346–2355 (2008).

12. J. Fostier and F. Olyslager, “Full-wave electromagnetic scattering at extremely large 2-D objects,” Electron. Lett. **45**, 245–246 (2009).
13. Ö. Ergül and L. Gürel, “A hierarchical partitioning strategy for an efficient parallelization of the multilevel fast multipole algorithm,” IEEE Trans. Antennas Propag. **57**, 1740–1750 (2009).
14. J. M. Taboada, L. Landesa, F. Obelleiro, J. L. Rodriguez, J. M. Bertolo, M. G. Araujo, J. C. Mourino, and A. Gomez, “High scalability FMM-FFT electromagnetic solver for supercomputer systems,” IEEE Trans. Antennas Propag. **51**, 21–28 (2009).
15. J. M. Taboada, M. G. Araujo, J. M. Bertolo, L. Landesa, F. Obelleiro, and J. L. Rodriguez, “MLFMA-FFT parallel algorithm for the solution of large-scale problems in electromagnetics,” Prog. Electromagn. Res. **105**, 15–30 (2010).
16. Ö. Ergül and L. Gürel, “Rigorous solutions of electromagnetics problems involving hundreds of millions of unknowns,” IEEE Trans. Antennas Propag. **53**, 18–26 (2011).
17. P. Ylä-Oijala and M. Taskinen, “Application of combined field integral equation for electromagnetic scattering by dielectric and composite objects,” IEEE Trans. Antennas Propag. **53**, 1168–1173 (2005).
18. P. Ylä-Oijala, “Numerical analysis of combined field integral equation formulations for electromagnetic scattering by dielectric and composite objects,” Prog. Electromagn. Res. C **3**, 19–43 (2008).
19. Ö. Ergül and L. Gürel, “Comparison of integral-equation formulations for the fast and accurate solution of scattering problems involving dielectric objects with the multilevel fast multipole algorithm,” IEEE Trans. Antennas Propag. **57**, 176–187 (2009).
20. Ö. Ergül and L. Gürel, “Efficient solution of the electric and magnetic current combined-field integral equation with the multilevel fast multipole algorithm and block-diagonal preconditioning,” Radio Sci. **44** (2009).
21. S. M. Rao, D. R. Wilton, and A. W. Glisson, “Electromagnetic scattering by surfaces of arbitrary shape,” IEEE Trans. Antennas Propag. **30**, 409–418 (1982).
22. Ö. Ergül and L. Gürel, “An efficient parallel implementation of the multilevel fast multipole algorithm for rigorous solutions of large-scale scattering problems,” in *International Symposium on Electromagnetic Theory* (IEEE, 2010), pp. 616–619.
23. Ö. Ergül and L. Gürel, “Advanced partitioning and communication strategies for the efficient parallelization of the multilevel fast multipole algorithm,” in *IEEE Antennas and Propagation Society International Symposium (APSURSI)* (IEEE, 2010), pp. 1–4.
24. Ö. Ergül, “Accurate and efficient solutions of electromagnetics problems with the multilevel fast multipole algorithm,” Ph.D thesis (Bilkent University, , 2009).
25. H. A. van der Vorst, “Bi-CGSTAB: A fast and smoothly converging variant of Bi-CG for the solution of nonsymmetric linear systems,” SIAM J. Sci. Stat. Comput. **13**, 631–644 (1992).